

https://dspace.org/

Design and development of proton exchange membrane (PEM) from synthetic rubber and carbon nanoballs for PEM fuel cell

Abdulkareem, Ambali Saka

2010-09-09
http://hdl.handle.net/10539/8632

Downloaded from a DSpace repository. https://dspace.org/

4.0 Production and Characterization of Carbon Nanoballs and other Nanoparticles

A series of experiments was carried out to synthesize carbon nanoparticles and membrane for fuel cell applications and the results obtained are reproducible. The swirled floating catalyst chemical vapour deposition (SFCCVD) reactor was used to synthesize the carbon nanoballs (CNBs) and other nanoparticles (CNPs), including carbon nanotubes (CNTs) and carbon nanofibres (CNFs). These nanoparticles are also characterized in this section.

4.1 Synthesis of Carbon Nanoparticles

During the process of producing CNBs, other nanoparticles are also produced. These carbon nanoparticles include mixtures of CNTs, CNFs, etc. Thus a series of developments have been made in synthesising CNBs through Catalytic Vapour Deposition (CVD) methods since its discovery as a possible route to the large scale and high quality production of CNPs (Conteau et al., 2003). In this research, CNTs were synthesized continuously in a swirled floating catalytic chemical vapour deposition reactor, using acetylene as a carbon source, ferrocene as a catalyst precursor and hydrogen and argon as carrier gases. The effects of various factors affecting the rate of CNTs production in a swirled floating catalyst chemical vapour deposition reactor were investigated. These factors are the pyrolysis temperature, acetylene flow rate and hydrogen flow rate. The quality of CNPs produced was analysed by the Transmission Electron Microscope (TEM), Higher Magnification Transmission Electron Microscope (HMTEM), Raman spectrometer and Thermo gravimetric analysis (TGA). In other words, to optimize the production of CNTs a series of experiments was conducted to synthesize CNPs at different operating conditions as mentioned above using the SFCCVD. The aim was thus to investigate and optimise the effects of these parameters on the production rate of CNPs. SFCCVD presents another form of conventional CVD

reactor and uses four gases as explained earlier in the experimental section (section 3.1). During the production process nitrogen gas was used to purge the equipment line and to detect any leakage in it. This gas was run until a maximum temperature of about 300^{o}C to prevent any possibility of high temperature reaction which might cause impurities in the products. To keep the system under an inert environment, Argon was then switched on to continue purging and also to act as a carrier gas and cool the equipment after production. The carbon source used in this work was acetylene gas while hydrogen was also used as a carrier gas and CNPs promoter. All gases used in the experiments were of analytical grade from Afrox. The decomposition of acetylene, which is the carbon source, occurs in the reaction zone of the reactor while all the gases move up the system against gravity. The design of SFCCVD is such that the swirled coil leads into the reactor to assist in providing a velocity profile that will create sufficient residence time within the reactor during production. During production, ferrocene, which is the catalyst precursor, was in a powder form, which evaporated and accompanied the gases into the reactor through the coil. These components react within the heating zone of the reactor to produce carbon products which evolve as black smoky particles and are collected in the two cyclones and reactor. Some of the products trapped in the reactor were also scrapped off.

The reaction of acetylene and ferrocene (the catalyst precursor) yielded a complex mixture of carbon nanoparticles such as CNFs, CNTs and amorphous carbon alongside CNBs, which are the product of interest under the conditions specified in Table 4.1.

Table 4.1: Production conditions of CNPs (Afolabi et al, 2007)

Flow rate of gases (ml/min)		**Carbon products composition at various temperatures (^oC)**			
Hydrogen	**Acetylene**	**900**	**950**	**1000**	**1050**
118	181	CNBs + CNTs	CNBs + CNTs	CNTs	CNTs
118	248	CNBs + CNTs	CNTs	CNTs	CNTs
118	308	CNBs + CNTs	CNTs	CNTs	CNTs
118	370	CNBs	CNTs	CNTs	CNTs
181	370	CNBs	CNTs	CNTs	CNTs
248	370	CNBs	CNTs	CNTs	CNFs

Figures 4.1 shows the TEM and HMTEM images of the products obtained at various production conditions as specified in Table 4.1

The product distribution of these carbon nanoparticles as observed from TEM images at various temperatures, acetylene flow rate and constant hydrogen flow rate of 181ml/min are presented in Tables 4.2 and 4.3. The iron content obtained in the product distribution was based on the percentage composition of ferrocene catalyst used in the synthesis of these nanoparticles.

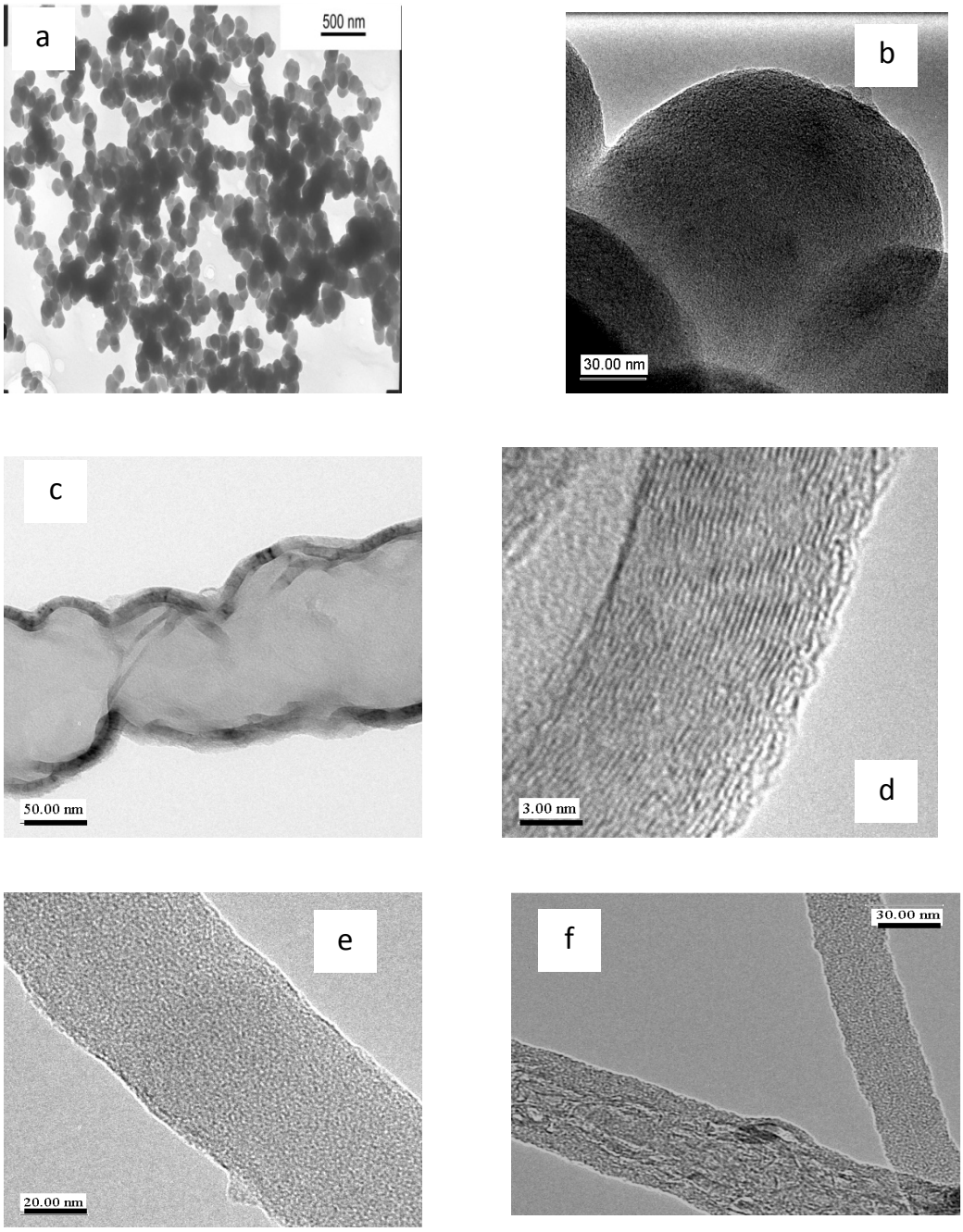


Figure 4.1: TEM images of carbon nanoparticles synthesised with SFCCVD at various conditions (a-b) TEM and HMTEM images of CNBs produced at 900°C, C_2H_2 = 370ml/min, H_2 = 181ml/min (c-d) TEM and HMTEM images of CNTs produced at 900°C, C_2H_2 = 370ml/min, H_2 = 181ml/min (e-f) TEM and HMTEM images of CNFs produced at 900°C, C_2H_2 = 370ml/min, H_2 = 181ml/min

Table 4.2: Product distribution of samples at hydrogen flow rate of 118ml/min and acetylene flow rate of 308ml/min

	Product distribution (%)		
Temperature (^{o}C)	**CNTs**	**CNBs**	**Fe**
900	7	92	1
950	94	4.5	1.5
1000	98.5	-	1.5
1050	99.5	-	1

Table 4.3: Product distribution of samples at hydrogen flow rate of 118ml/min and acetylene flow rate of 370ml/min

	Product distribution (%)		
Temperature (^{o}C)	**CNTs**	**CNBs**	**Fe**
900	9	89.5	1.5
950	96.5	1.5	2
1000	98.5	-	1.5
1050	99	-	1

Figure 4.2 (a – b) shows the product obtained with a hydrogen flow rate in the range of 181-248 ml/min and constant acetylene flow rate of 370 ml/min at the reaction temperature of 900^{o}C as shown in Table 4.1. These products contain agglomerate CNTs which are similar to the carbon nanoballs reported by Liu et al, (2002). The formation of these products could be attributed to the reaction temperature, and flow rates of acetylene (carbon source) and hydrogen employed during the production of these materials. It is observed that CNBs were produced at lower decomposition temperatures of the carbon

matrix from high flow rates of the carbon source and carrier gases. High flow rates of these gases created at low residence time within the reactor and the scattered catalyst particles within the carbon matrix formed different CNTs formation sites. These sites could not grow at low residence time and temperature; hence they culminated in CNBs formation. This is also a direct contrast from the findings obtained by Liu et al, (2002), where insufficient catalyst was attributed to CNBs production when the horizontal reactor, $Fe(CO)_5$ catalyst and pentane carbon source were used. It is also observed that these nanoballs contain negligible traces of iron impurities and no amorphous carbon, in line with the earlier explanation.

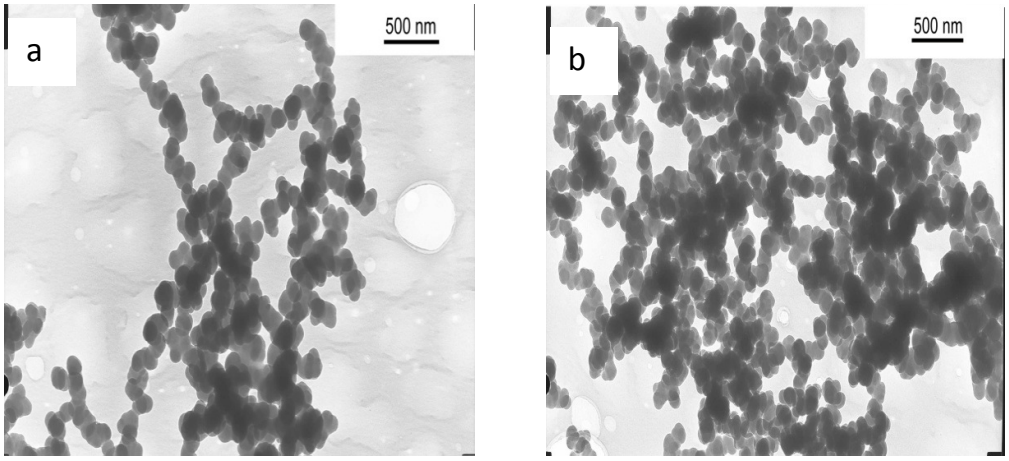


Figure 4.2 (a-b): TEM images of CNBs produced at (a) 900^{o}C, C_2H_2 = 370 ml/min, H_2 =181 ml/min (b) 900^{o}C, C_2H_2 = 370 ml/min, H_2 = 248 ml/min.

Figure 4.3 shows the TGA analysis of CNPs samples collected in the reactor, cyclone 1 and cyclone 2. Results reveal a drop in mass between 500-700^{o}C, which is a characteristic of the combustion of CNPs (Conteau et al, 2003). The TGA profile also shows that the CNPs produced contain impurities and some other materials that cause the

adulating in the profile. Figure 4.4 reveals the Raman spectroscopy of CNPs produced. The sample excitation was performed using 6mW of 514.5 nm light with a 1µm spot size. The integration time for the spectra collection was 2 minutes per acquisition. It is observed from Figure 4.4 that the G – peak splitting profiles and D-peak splitting frequencies of 1350 cm^{-1} and 1580 cm^{-1} confirm that samples contain CNPs. The Raman spectrum of CNPs produced at 950, 1000 and 1000^{o}C show the presence of two broad peaks at about 1350 cm^{-1} and 1580 cm^{-1} corresponding to the D-and G- bands of graphite respectively.

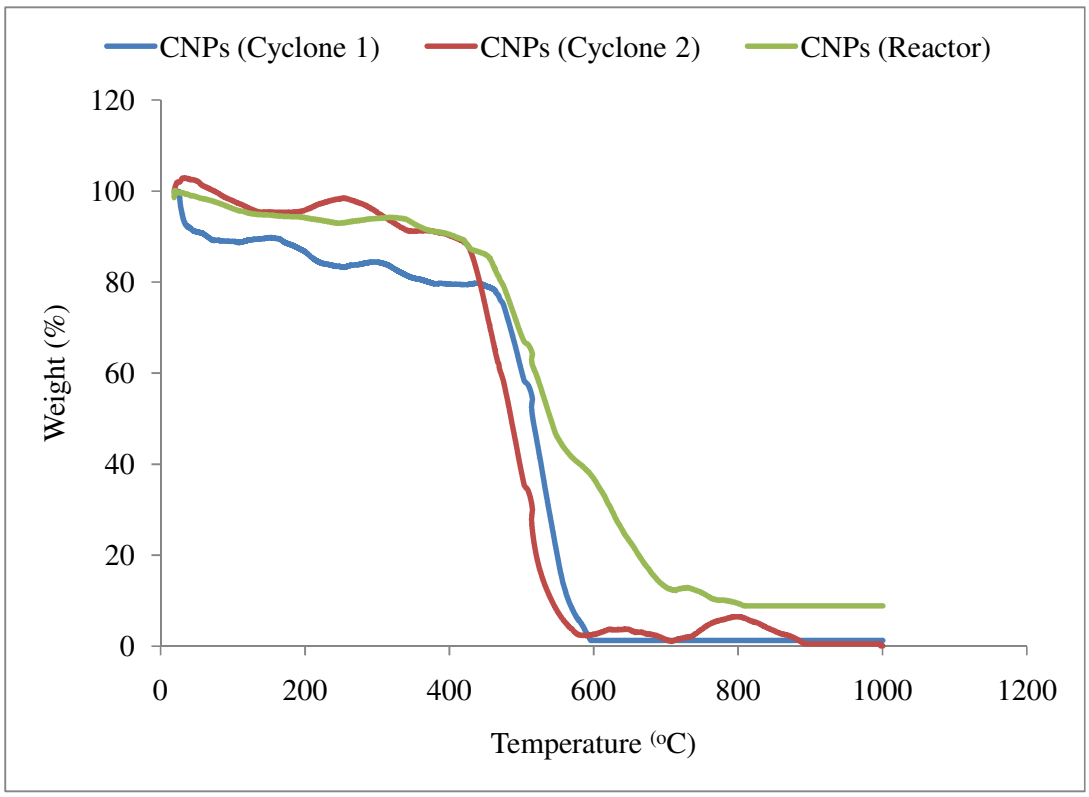


Figure 4.3: TGA profile of CNPs in an oxidizing air (atmosphere)

Raman spectra of the CNPs synthesized at different temperatures as shown in Figure 4.4 revealed that the $\frac{I_D}{G_D}$ ratios were 0.9, 0.85 and 0.80 at 950, 1000 and 1100^{o}C respectively. Raman spectra shown in Figure 4.3 also show that the intensity ratio of the

two bonds decreases with an increase in temperature, thus indicating that the degree of graphitization of the CNTs produced decreases with an increase in pyrolysis temperature, i.e. the value of $\frac{I_D}{G_D}$ equals 0.80 at 1100°C and is an indication that the degree of graphitization of the CNPs at 1100°C is low.

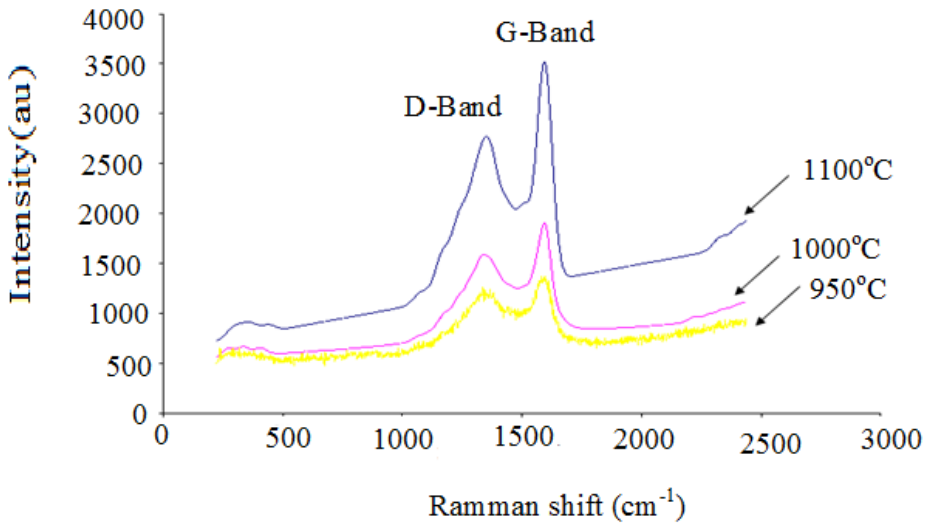


Figure 4.4: Raman spectrometer of the CNPs sample

The X-ray diffraction (XRD) pattern of the as-synthesized CNPs sample is shown in Figure 4.5 This pattern reveals a characteristic pattern of graphitised carbon which is similar to those reported by Zhang *et al.* (2005) and Kong and Zhang (2007). This pattern also indicates a high degree of crystallinity which suggests a low content of amorphous carbon and the presence of impurities drawn from the catalyst, usually iron particles (Wu *et al*, 2007). This observation made from the XRD process shows a marked difference from the results of the CVD process where the impurities from the catalyst employed in the pyrolysis process are always associated with the CNPs and require the adoption of various purification processes to remove them (Raymundo et al,

2005; Kumar and Ando, 2005; Wang et al, 2005). It could be inferred that the effective utilization of the ferrocene catalyst during the decomposition process would have resulted in a low content of iron impurities in the CNPs. Traces of amorphous carbon impurities, as stated above, are known to form as a result of insufficient catalyst used in the decomposition of acetylene. Only Argon/hydrogen (Moisala et al, 2006) was used to provide carrier gases and this eliminated the possibility of the high temperature oxidation of nitrogen which could introduce impurities in the products.

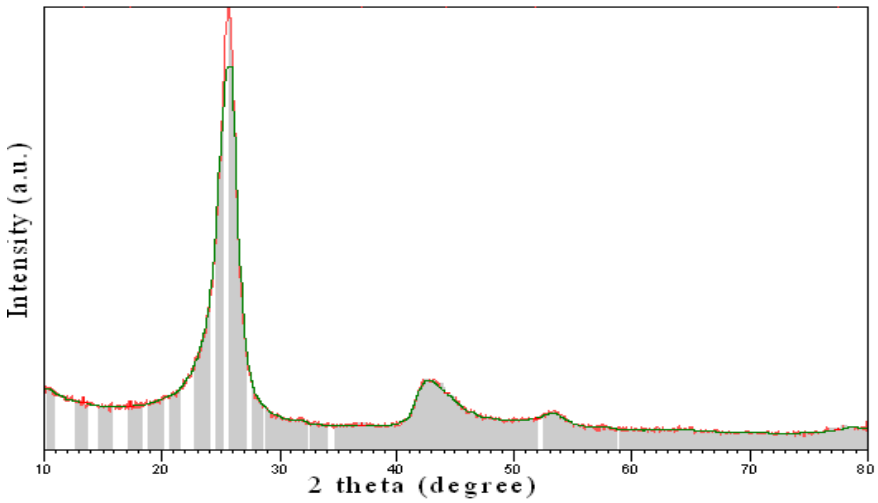


Figure 4.5: XRD pattern of CNPs sample.

Pure CNBs are required in this research as a reinforcing material for membrane synthesized from PSBR. It can be seen from Tables 4.2 and 4.3 that the synthesized CNPs contain a mixture of CNTs and CNFs and little impure iron content. Thus the synthesized CNPs are unsuitable for application in a membrane composite. Hence there is a need to synthesize pure CNBs free of impurities and other form of CNPs.

4.2 Non Catalytic Synthesis of Carbon Nanoballs

Carbon nanoballs were produced in a vertical SFCCVD reactor by the decomposition of acetylene without catalyst under different reaction conditions. The carbon soot formed was collected in both the reactor and the cyclones and analyzed with TEM, TGA, and Raman spectroscopy so as to evaluate the effect of the synthesis parameters on the yield and size (50 – 250 nm) of the CNBs formed. A typical example is described below.

Acetylene gas at a flow rate of 118 ml min^{-1} was passed through the reactor at 900^{o}C. The reaction was stopped after 4 min (gas flow changed to argon) and 1.4 grammes of soot were collected from both the reactor and the cyclones. TEM analysis of the soot from both the reactor and the cyclone was identical. A typical TEM image of the soot is shown in Figures 4.6 (a, c and e) and reveals that only carbon nanoballs (>99%) have been formed and that the nanoballs have an average diameter of 100 nm and show a narrow distribution range. The time that the acetylene spends in the reactor was estimated to be 33 seconds and within this short time the spheres were already accreted (Kang and Wang, 1996).

It is clear that at a high temperature, the carbon radicals formed in the gas phase in the reactor under these conditions nucleate and rapidly form solid spheres (Kang and Wang, 1996; Kang and Wang, 1997; Wang and Kang, 1996). The current mechanism for carbon nanoballs growth is consistent with the results found in earlier studies (Kang and Wang, 1996; Pol *et al*, 2004). The unusual phenomenon observed is that the carbon nanoballs are uniform in diameter. This suggests that nucleation commences at the inlet of the reactor, followed by the further rapid deposition of carbon onto the ball; and then further nucleation in the upper end of the reactor. It would appear that once the nuclei are

formed, the rate of carbon nanoball formation will then be determined by the acetylene concentration and the length of the reactor. However, it also appears that once the carbon nanoball has reached an optimum size, slight further growth takes place. The carbon nanoballs form a light and fluffy material, which is quite different in texture from spheres that were obtained from similar studies performed in a horizontal reactor (Mhlanga et al, 2007). In the horizontal reactor the carbon nanoballs were left in the reactor at a high temperature for a much longer time (15 – 120 min), resulting in secondary reactions occurring on the carbon nanoball perimeter. HMTEM analysis of the two types of carbon nanoballs is also a reflection of this difference. Carbon nanoballs obtained from a horizontal reactor have a distinctive core/shell structure whereas the spheres synthesized in the vertical reactor do not show this phenomenon (Figs. 4.6 b, d and f). As seen in the HMTEM image, the carbon nanoballs show a poorly graphitic structure with short (wavy) carbon layers closer and on top of each other. The surface area analysis of the spheres yielded a value of 7 m^2 $g^{-1,}$ indicating that the spheres had little or no porosity. CHN analysis of the spheres revealed that the materials contained carbon (~ 98%) and the remaining 2% comprised of hydrogen and possibly some oxygen.

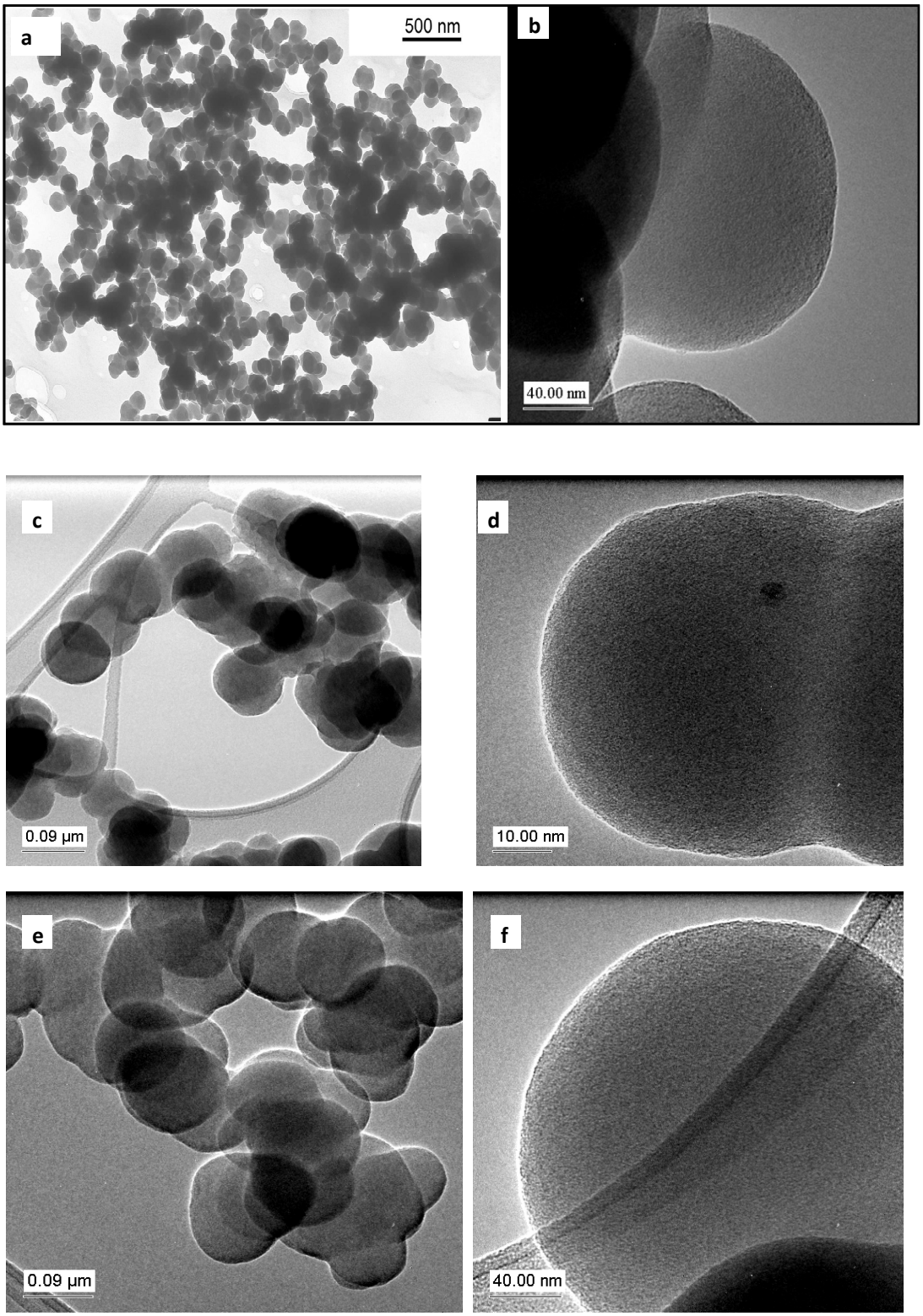


Figure 4.6: TEM image of carbon nanoballs produced by the SFCCVD technique at (a) 900°C (c) 950°C (e) 1000°C with C_2H_2 gas flow rate of 118 ml min^{-1}, (b, d f) Corresponding HMTEM image of the carbon nanoballs.

Upon heating the carbon nanoballs to 800^{o}C for 1 hour under nitrogen, the surface area increased to 15 m^2 g^{-1}. TGA analyses of both the as-prepared and post-heated samples are shown in Figure 4.7. The TGA data indicates a ca. 20% mass loss between 100 and 400^{o}C for the as-prepared carbon nanoballs, this is not observed after post treatment heating. The results are consistent with the surface area data and suggest that the carbon nanoballs prepared in the horizontal reactor contain readily removed species (either covalently or physically attached). When the carbon nanoballs were heated in a reactor under a continuous flow of argon, a black oily substance was generated inside the reactor. It is presumed that this oil may be associated with the 20% material lost in the TGA experiment. This grease was formed during the synthesis of the carbon nanoballs in a horizontal furnace. However in the horizontal CVD reactor, the grease was found at the exit end of the reactor (Mhlanga et al, 2007). It is nevertheless believed that this material found in both the horizontal and vertical reactors must be a precursor to the solid carbon nanoballs, albeit that the analysis of this material is yet to be undertaken.

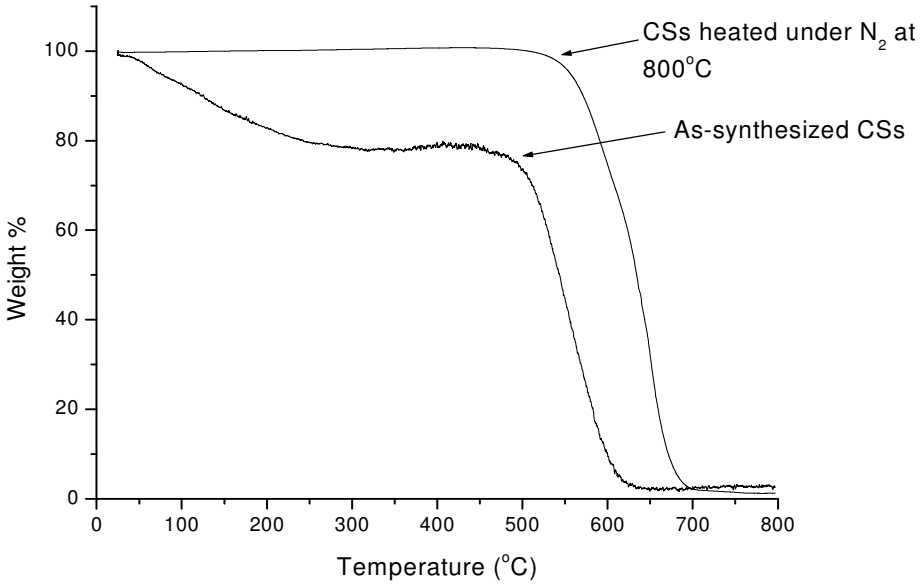


Figure 4.7: TGA profile of carbon nanoballs in an oxidizing (air) atmosphere.

HMTEM analysis of the post heated carbon spheres is shown in Figure 4.8 (a-b). The image reveals that these materials were made up of disordered arrays of graphene sheets of carbon. These layers are estimated to be 2 – 3 Angstroms apart and they form a spherical shape that typifies the carbon nanoballs. It can be observed that some of the balls are linked together (accreted) as shown by the arrows indicating the region where two balls have coalesced (Figure 4.8b). No outer core shell is again observed for the carbon nanoballs produced even after the post heating process (Mhlanga et al, 2007). Thus no significant change in the sphere morphology occurs in the post-heating process.

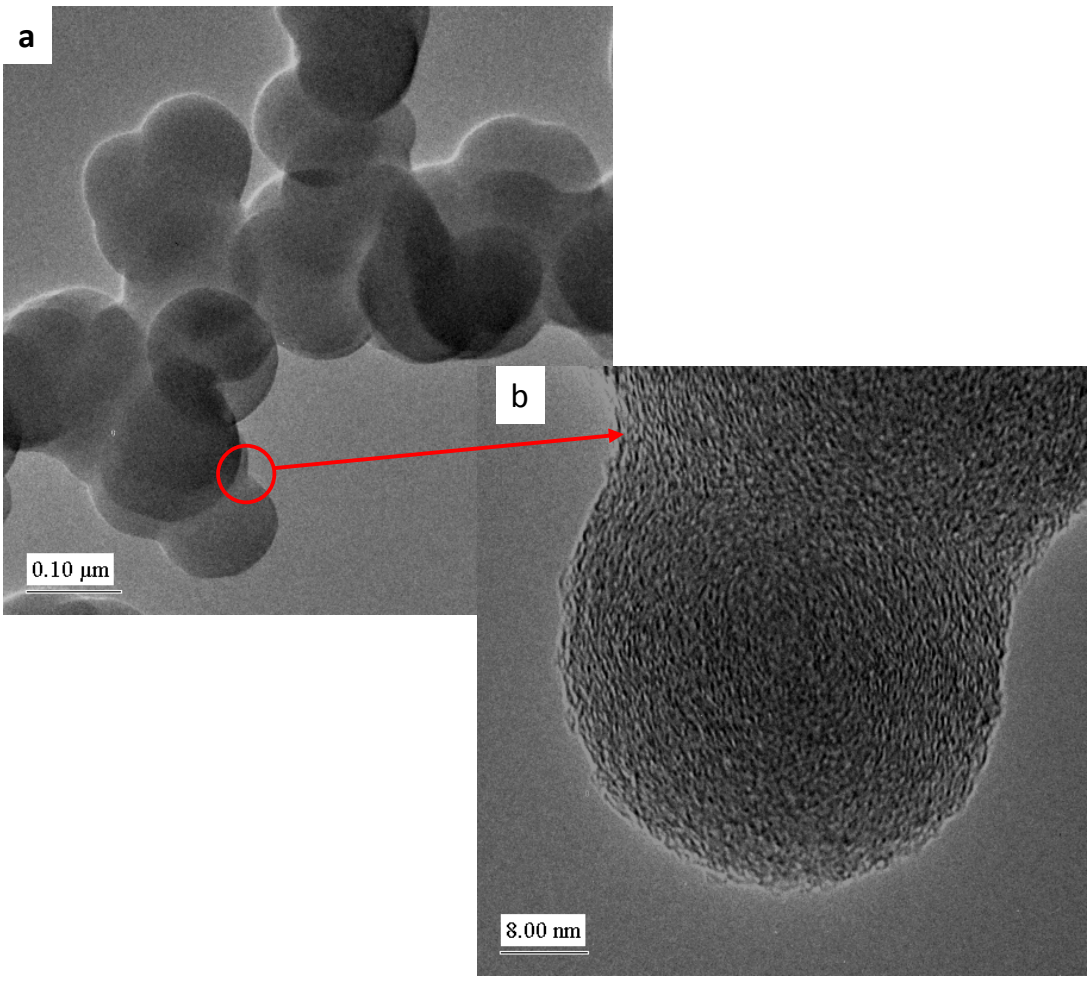


Figure 4.8 (a-b): HMTEM image of carbon nanoballs after heating at 800°C under nitrogen flow.

4.2.1 Effect of acetylene flow rate and temperature on CNBs synthesized

A series of experiment s were carried out to study the effect of acetylene flow rate and temperature on the production rate, size and structural morphology of the carbon nanoballs. The acetylene gas flow rate was varied from 70 – 370 ml min^{-1} while the pyrolysis temperatures used were 900, 950 and 1000°C respectively (Figure 4.9). As is evident from Figure 4.9, the rate of production of carbon nanoballs increased with the increasing flow rate of the feedstock at all pyrolysis temperatures. In general a higher temperature results in a modest increase in yield. A maximum production rate of ~ 0.35 g min^{-1} was obtained using an acetylene flow rate of 370 ml min^{-1} and a pyrolysis temperature of 1000^{o}C. This result is very close to the maximum production rate obtained in the synthesis of carbon nanoparticles when ferrocene catalyst precursor was used. The small effect of temperature suggests that above a certain minimum temperature the carbon species required to form the spheres are available in sufficient concentration without limiting the formation of the sphere.

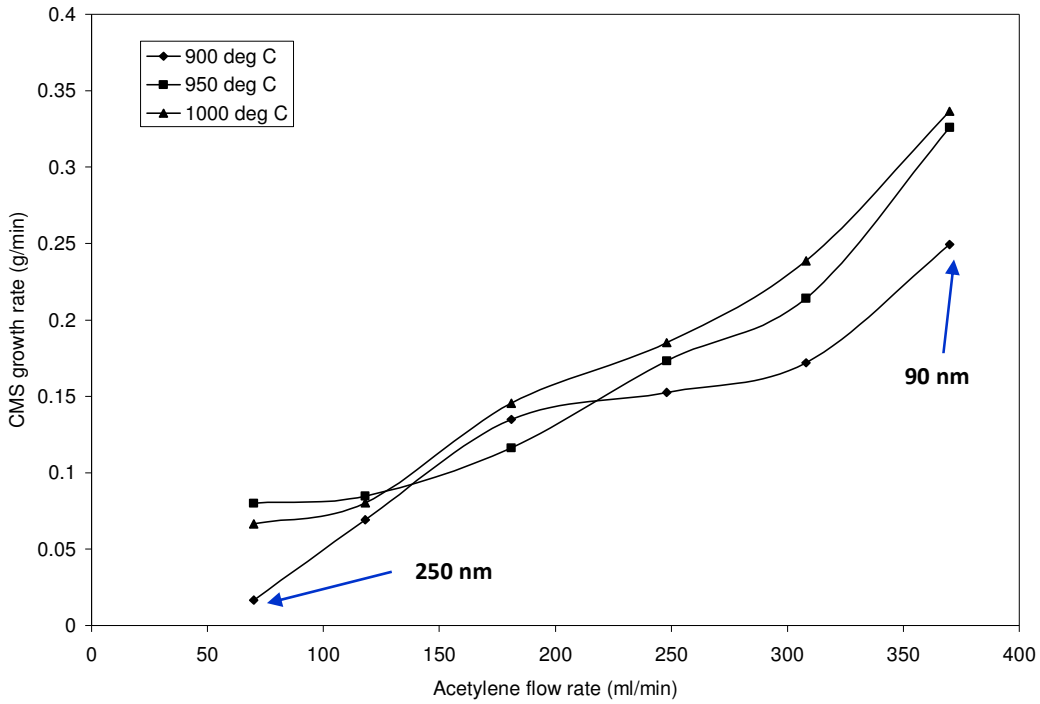


Figure 4.9: Rate of carbon nanoballs production at different temperatures and flow rate of acetylene.

Table 4.4 shows the sizes of carbon nanoballs obtained with different C_2H_2 gas flow rates at different pyrolysis temperatures. The results show that the C_2H_2 flow rate increases at 900^{o}C and the size of the carbon nanoballs decreases. This observation could be attributed to the residence time of C_2H_2 in the reactor. The residence time of the C_2H_2 will be higher at the lower C_2H_2 flow rate and this will allow the products to further accumulate the reactants before entering into the cyclone. These results also show that the carbon nanoballs size increases as the pyrolysis temperature increases. At a fixed C_2H_2 flow rate of 118 ml min^{-1}, the size of the carbon nanoballs increases from 120 nm to 150 nm as the pyrolysis temperature increases from 900 – 1000 ^{o}C.

Table 4.4: Diameters of carbon nanoballs produced at different temperatures and C_2H_2 gas flow rates.

Temperature (°C)	**C_2H_2 flow rate (ml min^{-1})**	**Average diameter (nm)**
900	70	250
900	118	120
900	181	100
900	248	90
950	118	100
1000	118	150

The effect of C_2H_2 dilution on the production rate of the carbon nanoballs, using an argon carrier gas, was also investigated at 1000°C. The argon flow rate varied from 70 – 370 ml min^{-1} while the C_2H_2 flow rate was kept at 181 ml/min. Dilution of the C_2H_2 with argon at the same flow rate was expected to lead to a lower yield of carbon products. However, at the increased total flow rate the data (Figure 4.10) shows that the rate of the formation of carbon nanoballs increases with dilution. Furthermore, the effect of the argon flow rate does not yield a linear trend and a drop in the rate of sphere formation rate is to be noted between the argon flow rates of 250 and 350 ml/min; this result is reproducible. As the flow rate of the carrier gas increased beyond 310 ml min^{-1}, the production rate of carbon nanoballs increased.

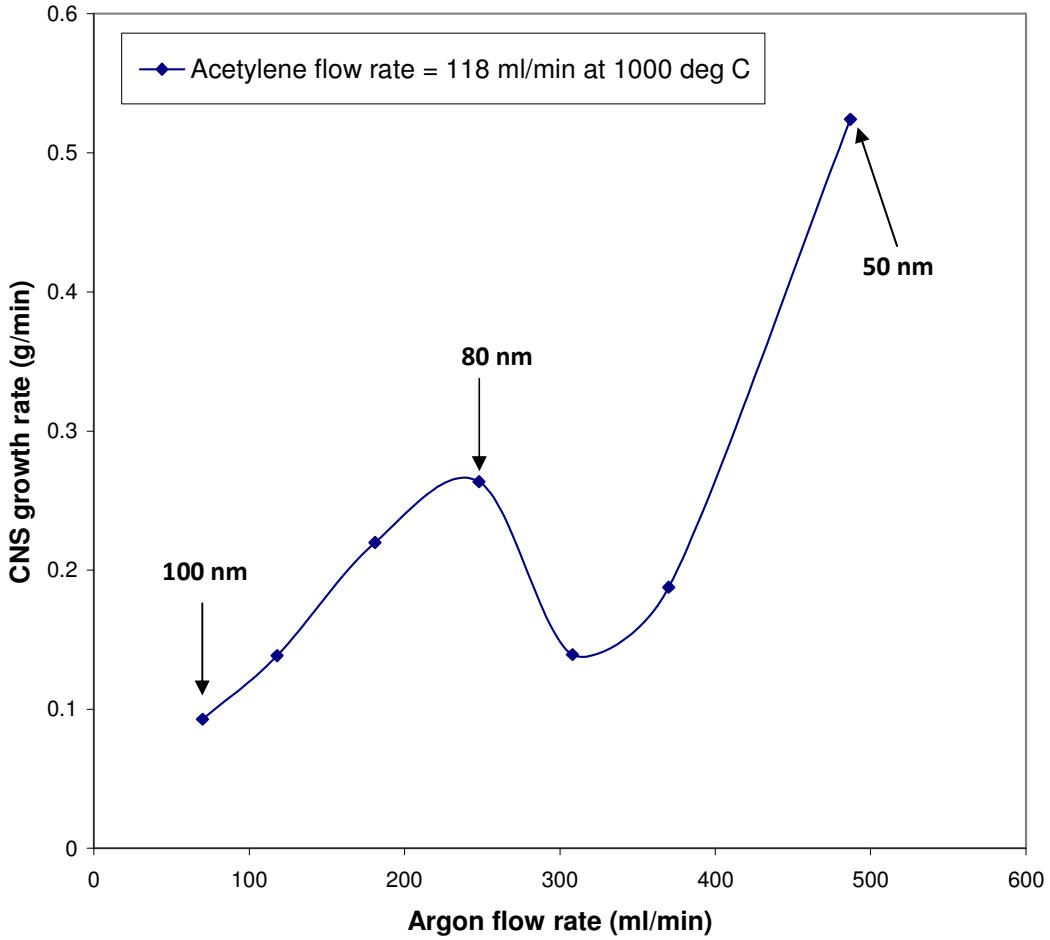


Figure 4.10: Effects of carrier gas on rate of carbon nanoballs production at constant flow rate of acetylene and temperature.

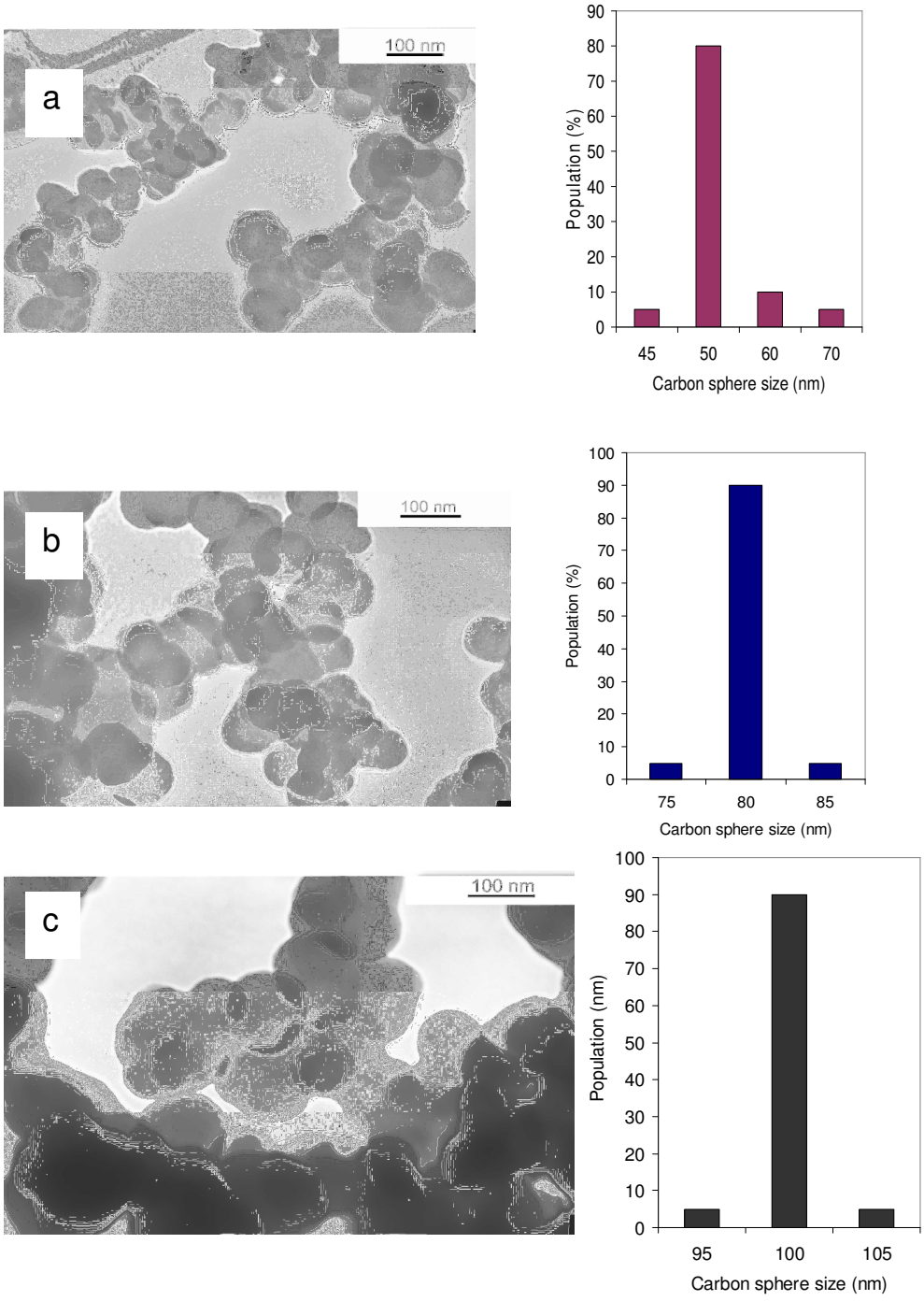


Figure 4.11 (a-c): TEM images of carbon nanoballs synthesized with Ar as carrier gas at a) 487 ml min^{-1}, b) 248 ml min^{-1}, and c) 70 ml min^{-1}. Histograms for the corresponding size distributions of the carbon nanoballs are shown on the right of the TEM images.

The size distributions of the carbon nanoballs products are shown in Figure 4.11. The spheres are quite uniform in size (> 80%) and possess similar features to the carbon nanoballs produced without Ar as a carrier gas.

Powder X – ray diffraction (PXRD) patterns of carbon nanoballs synthesized with and without carrier gas are shown in Figure 4.12. The pattern shows two peaks at 26^{o} and 45^{o} which correspond to carbon peaks (Zhang et al., 2005; Kong and Zhang, 2005). The PXRD pattern of both samples show that the peaks are broad; an observation that is attributed to low graphitization of the sample (Jin *et al* 2005). No differences were noted between the two PXRD patterns indicating that the argon carrier gas had no significant impact on the CNBs structure.

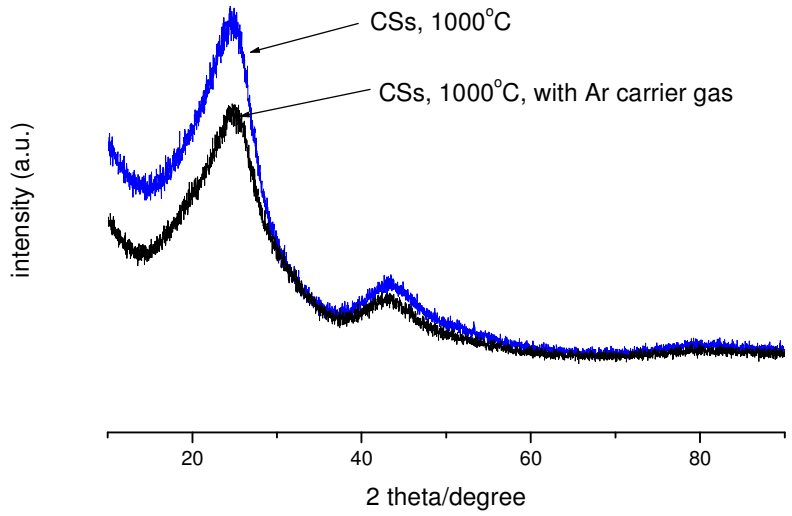


Figure 4.12: PXRD patterns of synthesized carbon nanoballs using the SFCCVD technique.

Figure 4.13 shows the Raman spectrum of carbon nanoballs produced at different temperatures (900, 950, 1000°C) and 118ml/min C_2H_2 constant flow rate. There are two

broad peaks at about 1350 cm^{-1} and 1580 cm^{-1} corresponding to the D- and G-bands of graphite respectively. The I_D/G_D ratios were ~ 0.65, 0.75 and 0.8 at 900, 950 and 1000°C respectively. The appearance of the bands is consistent with the presence of defects and disorder in the samples (Jin et al, 2005). Raman spectra also reveal that the intensity ratio of the two bands i.e. I_D/G_D increases with an increase in pyrolysis temperature. The value of I_D/G_D at 1000°C (~ 0.8) indicates that the degree of graphitization of the samples at this temperature is low.

The defectiveness of the samples produced at 950 and 1000°C, associated with the high values of I_D/I_G, suggests that the chemical reactivity of the samples should readily lead to the surface modification of the carbon nanoballs. This in turn could lead to the use of carbon nanoballs in various applications (e.g. catalysis) as suggested by Jin et al, (2005) and Xu et al, (2005). Furthermore, the low I_D/I_G value obtained at 900°C (~ 0.6) indicates the good crystallinity of these samples which is an indication of possible application of the carbon nanoballs in electronic environments.

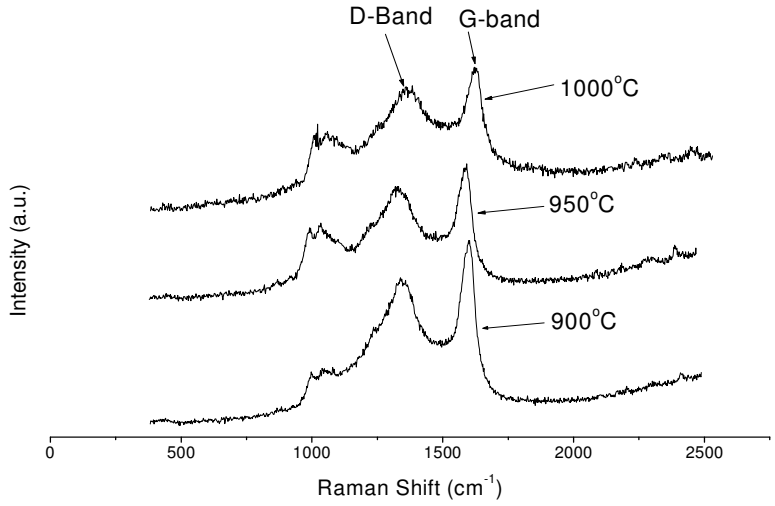


Figure 4.13: Raman spectra of carbon nanoballs.

A broad peak at ~ 1000 cm^{-1} was also observed in the Raman spectra of the carbon nanoballs. This peak disappears after the post heating of the carbon nanoballs as shown in Figure 4.14. The origin of this absorption observed before heat treatment is unknown at that stage (Pol *et al.*, 2004), but it can be attributed to the black oily substance generated inside the reactor when the carbon nanoballs are heated under a continuous flow of argon. Raman spectra of the heat treated samples also revealed that the $\frac{I_D}{I_G}$ ratios were affected: the ratio after the heat treatment was ~ 0.86, 0.91 and 0.94 at 900, 950 and 1000°C respectively.

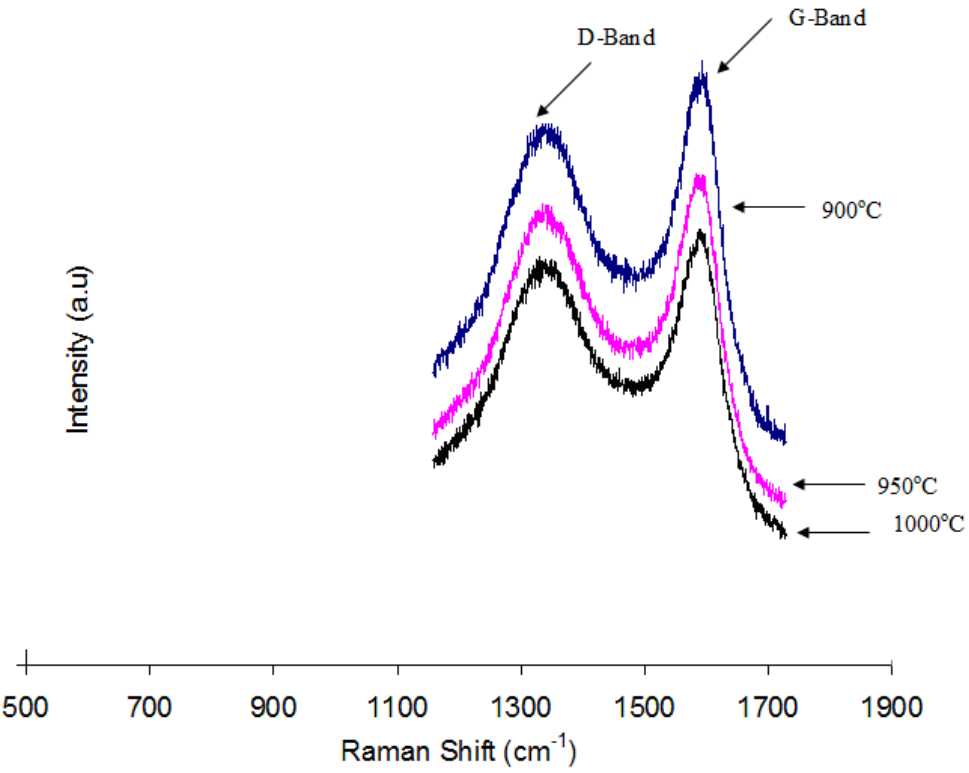


Figure 4.14: Raman spectra of carbon nanoballs after heat treatment